International Journal of Heat and Technology
Vol. 44, No. 1, February, 2026, pp. 167-177
Journal homepage: http://iieta.org/journals/ijht

Influence of the Longitudinal Gap Between Containers on the Wind Forces on a Container Ship

Djawad S. Berrezoug*, Mohamed Bouzit, Fayçal Chergui

Laboratory of Maritime Sciences and Engineering (LSIM), University of Science and Technology of Oran Mohamed Boudiaf, Oran 31000, Algeria

Corresponding Author Email: djawadsoufiane.berrezoug@univ-usto.dz

https://doi.org/10.18280/ijht.440114

Received: 22 November 2025
Revised: 19 January 2026
Accepted: 26 January 2026
Available online: 28 February 2026

Keywords:
aerodynamic force, air resistance, longitudinal gap

ABSTRACT

A numerical 3D simulation of turbulent airflow is carried out over a generic model of a container ship to study the effects of the longitudinal gap between containers (dx = 0, 15, 20, and 25 mm), the aerodynamic force Fx using a computational fluid dynamics (CFD) code. For validation, the profile of velocity and the aerodynamic coefficient of force are compared with those obtained by numerical and experimental results made by MOAT and W.D. Janssen, respectively, showing a similar agreement. Reducing the aerodynamic force on the ship leads to a decrease in total force and, consequently, a reduction in fuel consumption. This study confirms that the gap flows have a significant effect on the air resistance of the container ship; as a result, there is a reduction of the aerodynamic force Fx. It has been demonstrated that the gap flow decreases the air resistance acting on the container ship by up to 11.49 % of the aerodynamic force Fx when the longitudinal gap is 25 mm, compared to a dx = 0.

1. INTRODUCTION

In order to optimize ship performance, it is essential to minimize total resistance as much as possible. The aerodynamic resistance constitutes 3 to 5% of the total resistance of the ship; however, in the case of a container ship, the extensive projected surfaces facing the relative wind lead to an increase in aerodynamic drag, which represents about 2–10% of the overall resistance [1].

Grlj et al. [2] analyzed how various container arrangements influence aerodynamic resistance and found that air resistance represents between 3.5% and 5.8% of the overall resistance, depending on the configuration.

On the impact of container arrangement on aerodynamic forces, Andersen [3] studied the influence of container configurations on a scale model of a container ship. The numerical and experimental study demonstrated that the magnitude of the wind force depends on the container configuration. Also, Deng et al. [4] conducted a numerical investigation on the effect of stacking configuration and forecastle fairing on the aerodynamic drag of large container ships. Their results indicated that aerodynamic resistance strongly depends on the container arrangement, with certain stacking configurations leading to noticeable drag reduction. Additionally, the study demonstrated that optimized forecastle fairing geometries can significantly improve aerodynamic performance, achieving a drag reduction of up to 20.85%.

Qiao et al. [5] experimentally and numerically investigated the wind load characteristics of a container ship under different container stacking modes. The results showed that the conventional stacking configuration leads to lower aerodynamic loads and resistance.

Kim et al. [6] conducted studies on the design and performance evaluation of superstructure modifications aimed at reducing air drag on container ships.

Studies that showed the influence of gaps on aerodynamic forces include Watanabe et al. [7], who studied the effects of transversal gaps between containers on the air resistance of a container ship. Other geometric modifications to the containers and the front of the ship were also examined to reduce aerodynamic resistance; they found that the bow deck can reduce air resistance by up to 30%. Nguyen et al. [8] numerically studied airflow over a large container ship and analyzed the effects of transversal gaps on air resistance for different wind angles. They concluded that when the gap flow over the containers was covered, air resistance was reduced for angles between 30° and 60°. Furthermore, Nguyen and Ikeda [9] studied the effects of covering the spacing between containers on aerodynamic forces and concluded that wind force can be reduced by 27% to 30% for full side gap covers and by 18% to 19% for partial gap covers. Nguyen et al. [10] studied airflow over container ships theoretically and experimentally using a side cover, a center wall, and a dome at the bow deck. They concluded that side covers and centre walls reduce wind resistance in head and bow oblique winds, while the dome can reduce air resistance by up to 30%.

A simplified geometric representation of merchant ships was suggested by Moat in the form of a generic model. An experimental and numerical study was conducted by Moat to investigate the variations of wind speed above the superstructure on merchant vessels, such as tankers and container ships. Within the framework of voluntary observing

ships [11, 12]. Janssen et al. [13] compared several simplified geometric representations of a container ship with experimental results and demonstrated that the prediction error of the aerodynamic force decreases from approximately 37.9% for simplified models to about 5.9% for the most detailed configuration.

Research on the aerodynamic interaction between the hull and superstructure showed that He et al. [14] investigated the effects of the accommodation, the hull, and the hull combined with accommodation on the drag force of a container ship. They concluded that, to reduce drag force, interactions between the hull and the accommodation must be minimized. Majdiana and Azarsina [1] conducted simulations with ANSYS CFX to evaluate the aerodynamic forces on a container ship. They found that variations in the aft superstructure configuration significantly affect air resistance, particularly due to the height of the first bay located just behind the superstructure. Also, Seok and Park [15] investigated the ship's total drag with and without the superstructure for different Froude numbers (Fn). They showed that the superstructure slightly increases air resistance, particularly at low speeds.

Wang et al. [16] performed numerical simulations and experiments to investigate the effects of wind and wave forces on container ships. Their results showed that the combined action of wind and waves led to a higher ship resistance, exceeding the sum of the individual contributions.

Other studies on airflow over ships include O'Sullivan et al. [17], who investigated airflow distortion around research vessels using computational fluid dynamics (CFD) based on previously obtained experimental data, demonstrating how wind flow distortions can be analyzed through numerical simulations. Ricci et al. [18] conducted CFD simulations of wind forces acting on ships moored in port environments, showing the significant impact of surrounding structures on wind loads acting on the hull.

For the use of the ANSYS CFX code to study the airflow over a container ship, we refer to the previous studies [1, 19]. Majidian and Azarsina [19] numerically investigated the airflow around a container ship subjected to oblique winds (0°–40°) using the ANSYS CFX code. Four different approaches were tested to model the air–sea interface. Their results demonstrated the suitability of the CFX solver for simulating wind effects on container ships.

While several studies investigated the influence of container arrangements or superstructure modifications on air resistance, most focused on transverse gaps and did not consider longitudinal gaps in detail. Therefore, this study addresses the remaining research gap by focusing on the influence of longitudinal gaps.

This numerical study investigated the effects of longitudinal gaps between containers on the aerodynamic forces on the ship. Initially, a mesh test was carried out, followed by a validation of the numerical results regarding the velocity variation above the superstructure of a generic container ship model and the aerodynamic force coefficients Cx and Cy of a simple block representing a simplified model of a container ship proposed by Moat [12] and Janssen et al. [13], respectively. Finally, a numerical study was conducted to assess the effects of the longitudinal gaps (dx = 15 mm, dx = 20 mm, and dx = 25 mm) between containers on the aerodynamic forces.

2. NUMERICAL DOMAIN

The numerical domain consists of a container ship, 170 m in length, modeled at a 1:46 scale, and positioned centrally in width and 3 m from the inlet in length within a computational domain measuring 9.7 × 1.5 × 1.265 meters, ensuring sufficient clearance on all sides. In this study, the original generic container block model was modified to investigate the variation of dx = 0, 15, 20, and 25 mm. The block is composed of 8 containers in width and 11 containers in length for the 40-foot container model. The dimensions of the block are 3014 mm in length, 424 mm in width, and 188 mm in height (see Figure 1). Four configurations (dx = 0, 15, 20, and 25 mm) are considered.

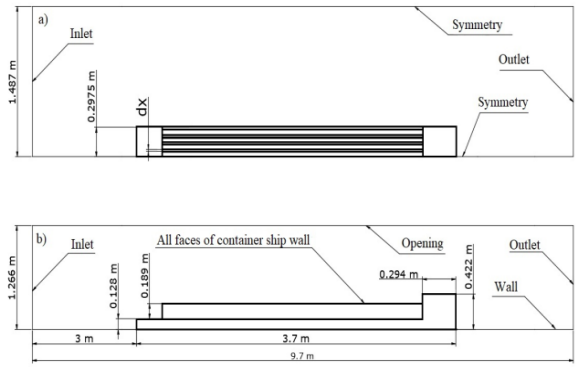

Figure 1. Side and plan representations of the computational domain for the container ship

Another simulation was used to validate the force coefficients C_x and C_Y with the experimental and numerical results of Janssen et al. [13] (Figure 2).

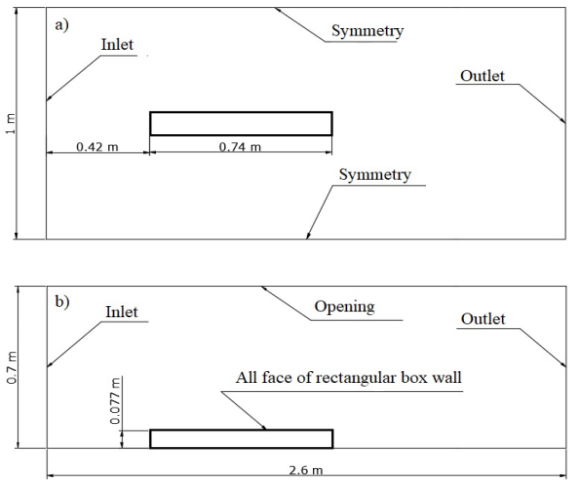

Figure 2. Side and plan representations of the computational domain of the simplified representation of the container ship (rectangular box)

3. BOUNDARY CONDITION AND MESH DESCRIPTION

Boundary conditions are applied to all boundaries of the computational domain. At the inflow boundary, a constant velocity profile of 7 m/s is imposed. The turbulent kinetic energy (k) and dissipation rate (ε) profiles are defined using uniform distributions, corresponding to a free-stream

turbulence intensity of 5% and a turbulent-to-molecular viscosity ratio of 50%. At the outflow boundary, all flow variable gradients along the streamwise direction are set to zero. Wall boundary conditions are applied to all container walls, including the bottom. Symmetry boundary conditions are applied to the north and south walls, while the top boundary is treated as an opening.

Since the dimensions are important, implying an increase in the number of nodes (2.5 m), and since the domain is symmetrical, we use half of the domain (1.5 m), which gives a similar result [1]. During our study, we studied the influence of the longitudinal gap between containers on the aerodynamic force of the ship. Four configurations are taken, namely dx = 0, dx = 15, dx = 20, and dx = 25 mm. The simulation dx = 0 mm is taken as a reference for comparison.

The mesh used is a structured and uniform mesh on the domain generated by the commercial CFX code (Figure 3). A mesh test was carried out for different meshes ranging from 14, 12, 10, 9, 8, and 7 meshes, summarized in the following table (Table 1). For simulations employing the k–ε turbulence model with standard wall functions in ANSYS CFX, the near-wall mesh was designed such that the dimensionless wall distance Y^+ of the first cell remained between 30 and 300. This ensures that the first mesh point lies within the logarithmic region of the turbulent boundary layer, where the wall function assumptions are valid. We can see the work of Ariff et al. [20] for the wall Y+ approach.

Table 1. Variation of the force Fx as a function of the mesh

Mesh Height	Number of Nodes	Y^+	Fx (N)
14	2719304	490	4.167904
12	3655083	427	4.206383
10	5363355	364	4.196518
9	7290420	334	4.256995
8	8228740	307	4.256995
7	12539721	275	4.280715

The results found show that the force Fx, and therefore the frontal force, shows a slight variation depending on the mesh used. And to verify the k-ε model, we use a uniform mesh of 7 for the different configurations studied.

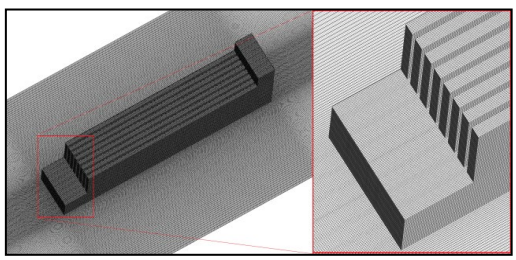

Figure 3. Computational grid mesh of the container ship for dx = 25 mm

4. MATHEMATICAL FORMULATION

In this study, the steady Reynolds-Averaged Navier–Stokes (RANS) equations were solved to compute the flow field. The governing continuity and momentum equations for incompressible flow are expressed in Eq. (1) and Eq. (2).

$$\frac{\partial \rho \bar{u}_i}{\partial x_i} = 0 \tag{1}$$

$$\frac{\partial\left(\rho \bar{u}_i \bar{u}_i + \rho \overline{u_i' u_j'}\right)}{\partial x_j} = -\frac{\partial \bar{p}}{\partial x_i} + \frac{\partial \overline{\tau_{ij}}}{\partial x_j} \tag{2}$$

where, ρ is density $\bar{U}_i$ is average Cartesian components of velocity vectors, $\rho \overline{u_i' u_j'}$ are Reynolds stress and $\bar{p}$ is the mean pressure, $\overline{\tau_{ij}}$ are the mean viscous stress tensor components.

$$\bar{\tau}_{ij} = \mu\left(\frac{\partial \bar{u}_i}{\partial \bar{x}_j} + \frac{\partial \bar{u}_i}{\partial \bar{x}_j}\right) \tag{3}$$

where, μ is the dynamic viscosity.

5. WIND RESISTANCE

The aerodynamic coefficients are defined as Eqs. (4) and (5):

$$C_x = \frac{F_x}{\frac{1}{2}\rho_{air} U^2 A_F} \tag{4}$$

$$C_y = \frac{F_y}{\frac{1}{2}\rho_{air} U^2 A_S} \tag{5}$$

where, C_x and C_y are the resistance coefficients in x and y directions, respectively.

F_x and F_y are longitudinal and transverse forces in x.

and y direction, respectively.

ρ_{air} is the air density (Kg/m^3).

U is uniform air velocity (m/s).

A_F and A_S are the frontal projected and sides projected areas (m^2), respectively.

6. COMPUTATIONAL FLUID DYNAMICS VALIDATION STUDY

For the validation, we compared CFD results obtained with the configuration of Moat for generic scaled models of container ships [12]. The mesh grid used includes 10,809,246 nodes with a Y^+ value less than 277.

Figure 4 illustrates the normalized wind velocity profiles along the vertical direction at various dimensionless downstream locations (x/step height) above the bridge. The vertical coordinate is represented by the normalized height (z/step height).

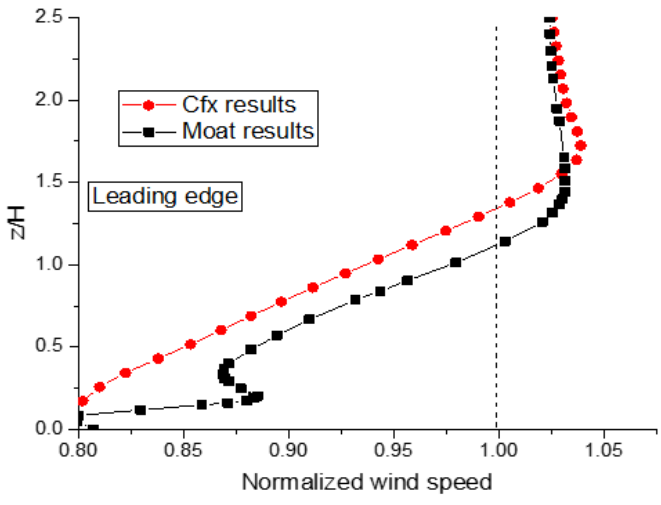

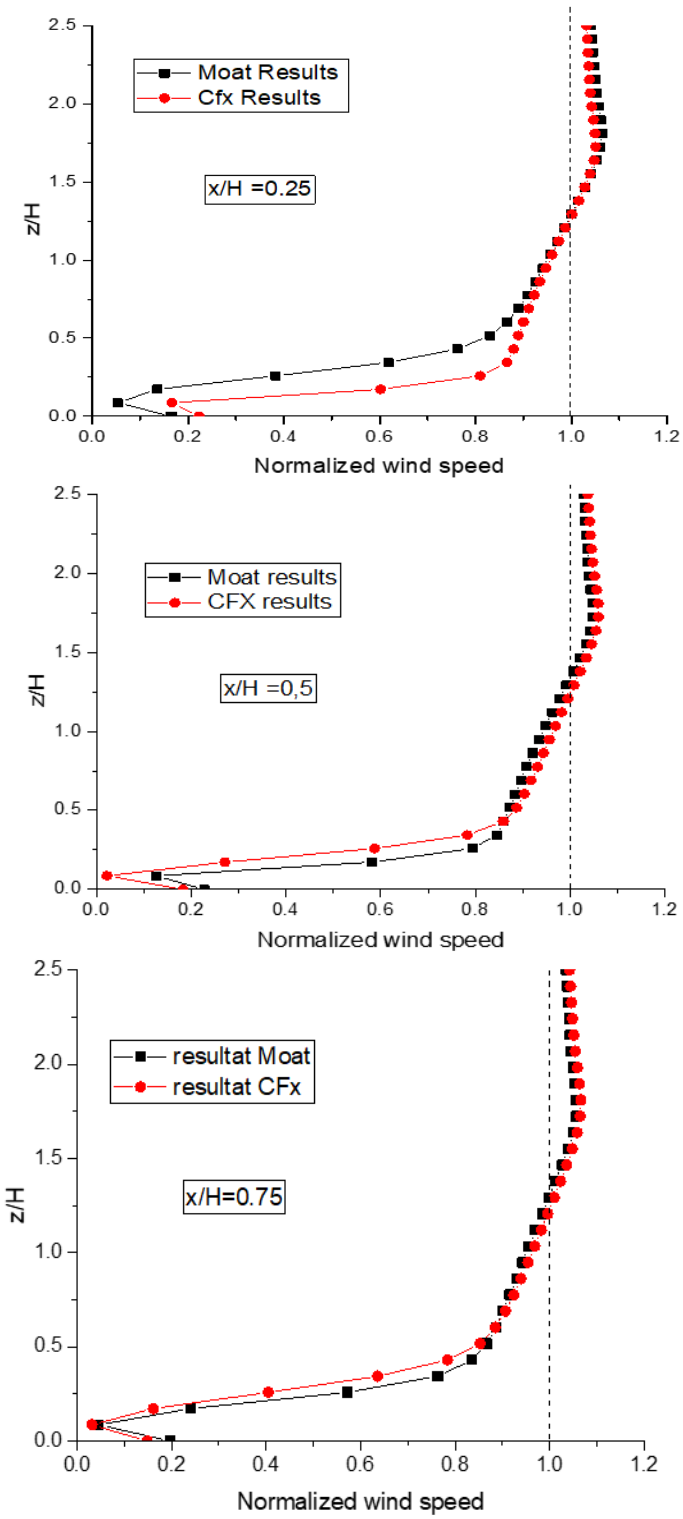

Figure 4. CFD-predicted vertical distributions of normalized wind velocity at the leading edge and at downstream positions x/H = 0.25, 0.50, and 0.75

The profiles are reported at normalized streamwise positions x/H equal to 0 (leading edge), 0.25, 0.50, and 0.75. The dashed line represents a normalized velocity of 1.0, corresponding to the free-stream condition. The CFD results obtained are in good agreement with the CFD results of Moat, except in the depression zones, where the speeds reach their values at slightly higher elevations.

For the validation of the Cx and Cy, we compared our results with those obtained by Janssen et al. [13] using a rectangular box model as a simplified representation of a container ship. CFD results obtained are in good agreement with the CFD results of Janssen et al. [13] (see Figure 5).

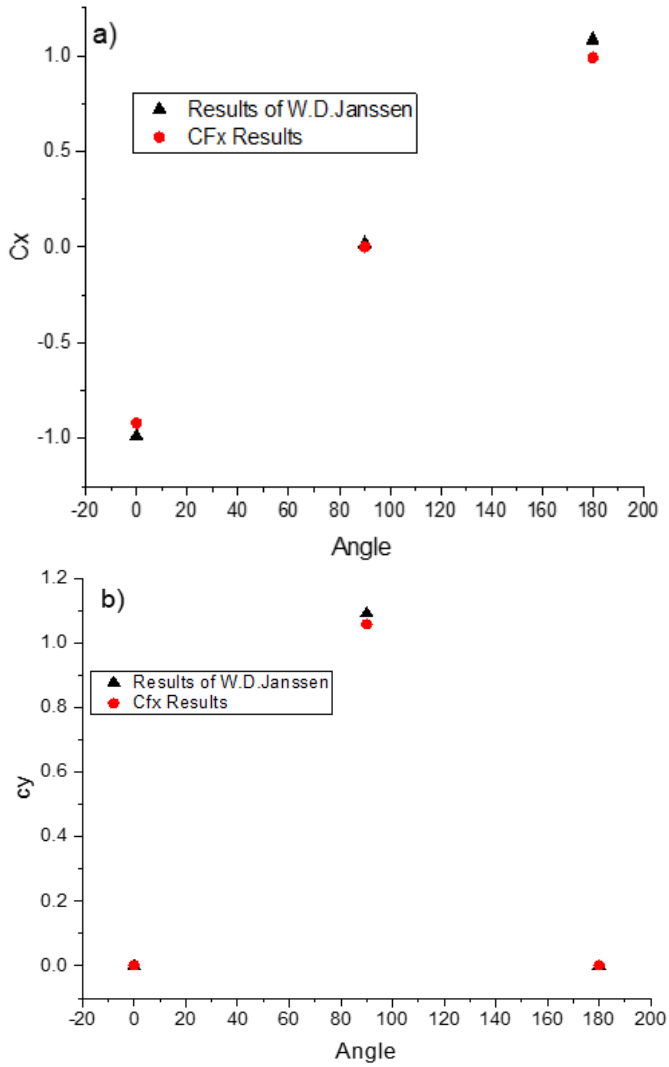

Figure 5. Numerical force coefficients on the ship as a function of wind angle: (a) C_X, (b) C_Y

7. RESULTS AND DISCUSSION

7.1 Pressure and force distribution for a longitudinal plan

Figure 6 shows the pressure distribution on the container hip. For dx = 0, Figure 6(a), we note that the pressure is progressively greater on the forward face of the first container block, at the bow of the hull, and finally on the front surface of the superstructure. The pressure distribution on the container ship for a uniform profile at the inlet is the same as that found by Hyounggil Park et al. [21]. We note that the pressure on the superstructure tends to decrease as dx increases.

Figure 7 shows the force distribution on the container ship. For dx = 0 (Figure 7(a)), it is observed that the force gradually increases on the front face of the containers, then at the bow of the hull, and finally on the front surface of the superstructure. It is also noted that the force on the superstructure tends to decrease as dx increases.

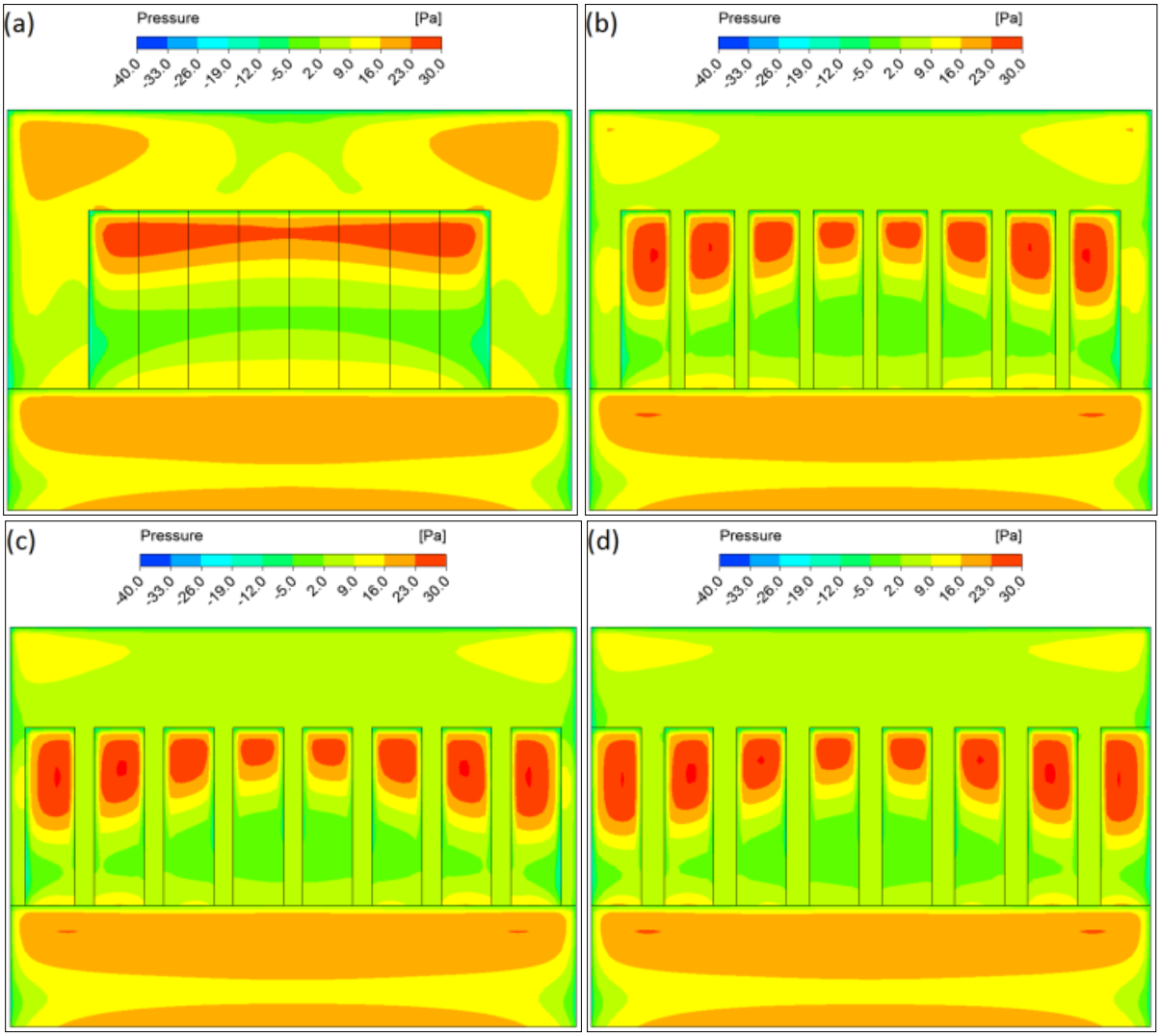

Figure 6. Pressure distribution for a longitudinal gap between containers: (a) dx = 0 mm, (b) dx = 15 mm, (c) dx = 20 mm, and (d) dx = 25 mm on a container ship

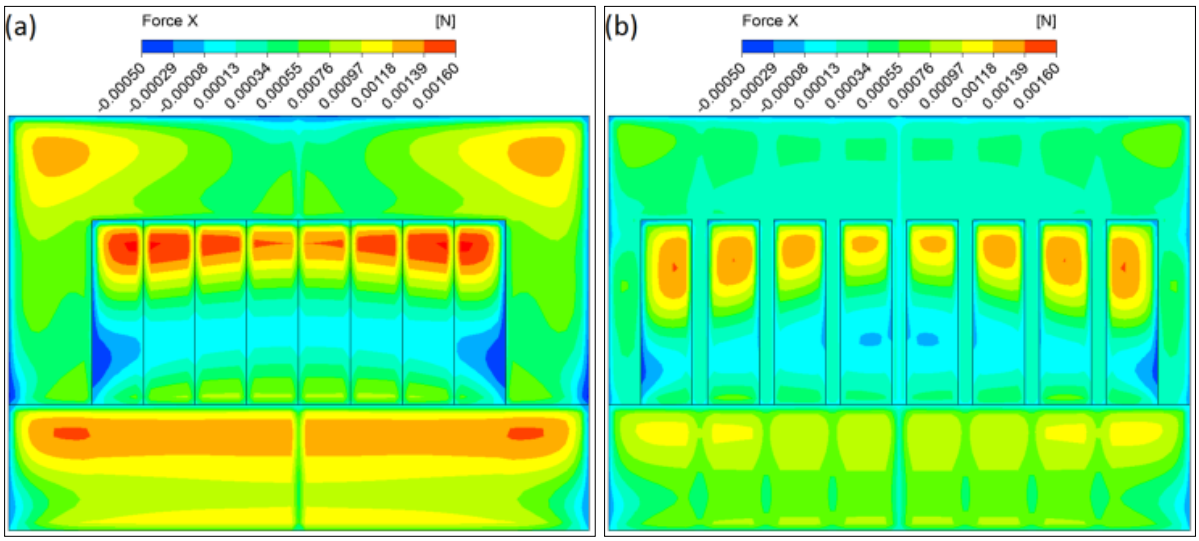

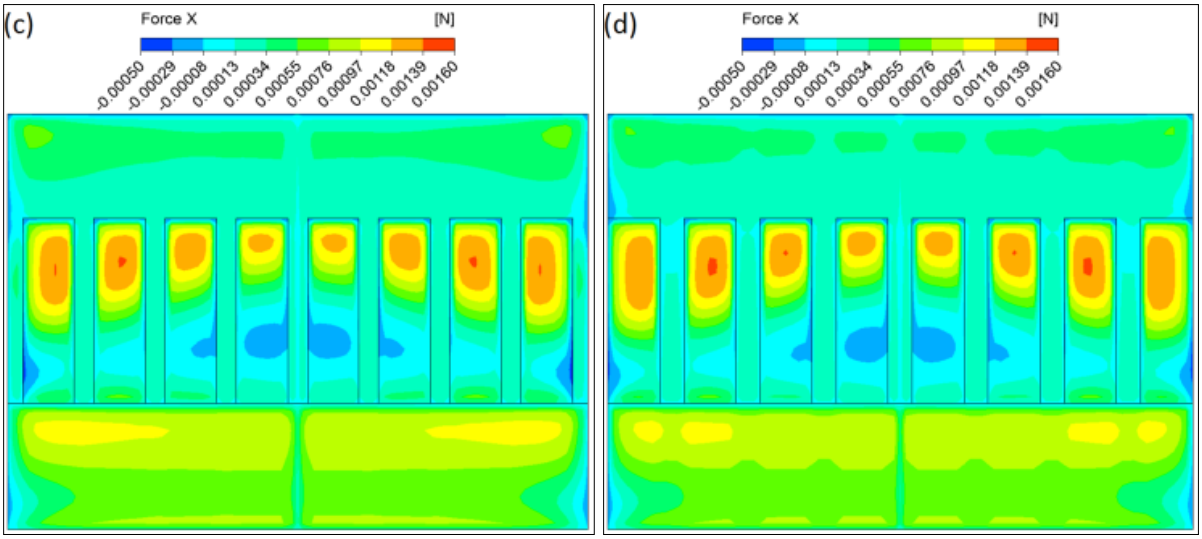

Figure 7. Force distribution for a longitudinal gap between containers: (a) dx = 0 mm, (b) dx = 15 mm, (c) dx = 20 mm, and (d) dx = 25 mm on a container ship

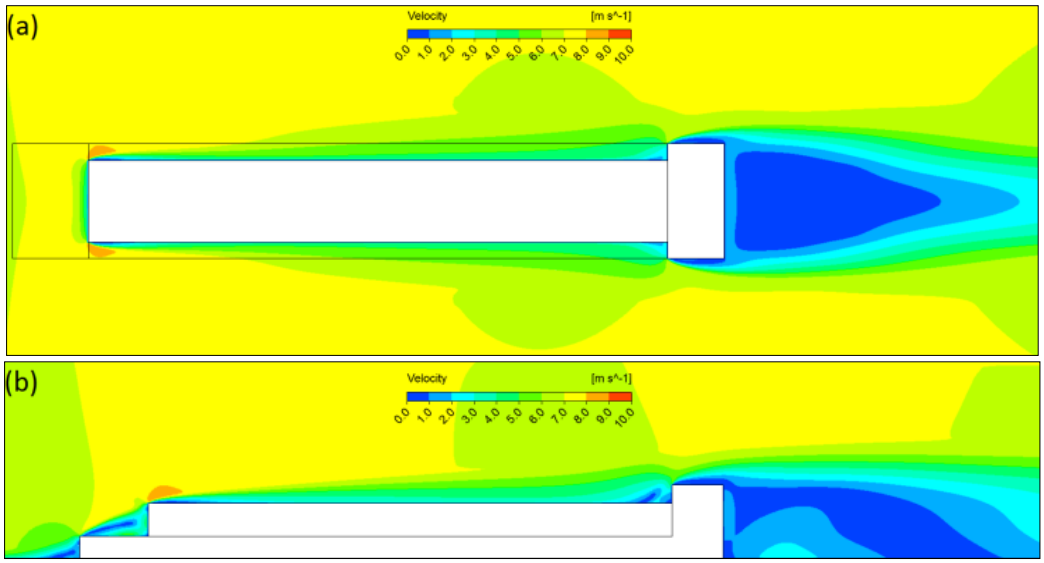

Figure 8. Velocity distribution on the longitudinal (z = 0.222 m) and transverse (y = 0) planes of the container ship for longitudinal container gaps dx = 0 mm

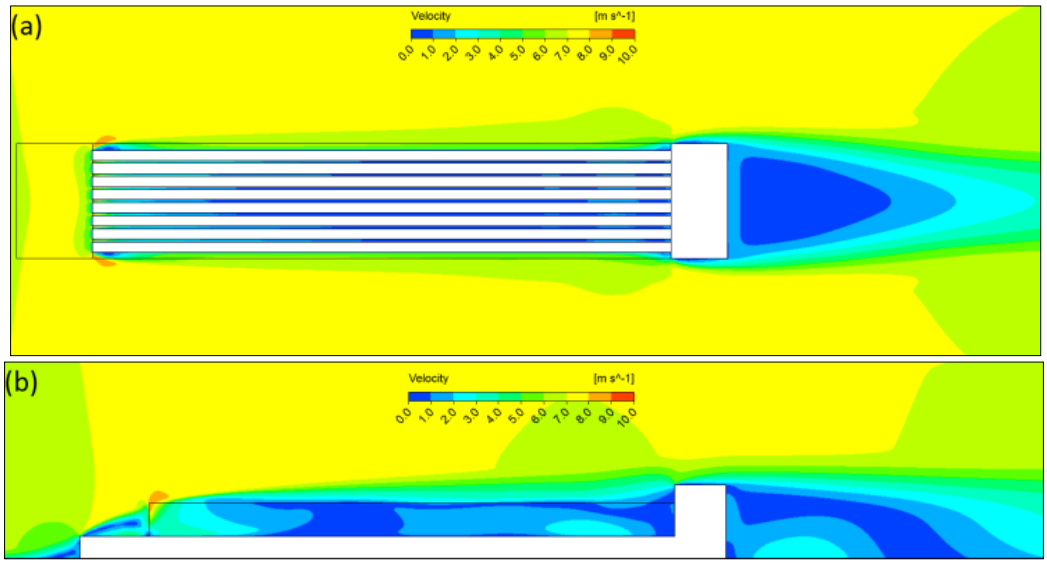

Figure 9. Velocity distribution on the longitudinal (z = 0.222 m) and transverse (y = 0) planes of the container ship for longitudinal container gaps dx = 15 mm

7.2 Velocity distribution for a longitudinal and transverse planes

Figures 8 to 11 show the velocity distribution on the longitudinal and transverse planes of the container ship. A wake is observed forming over the containers and along the sides of the ship. As dx increases, the wake thickness tends to decrease. It is also observed that flow begins to pass through the gaps between the containers starting at dx = 15 mm. It is also observed that airflow tends to penetrate between the containers, although at a relatively low velocity.

7.3 Velocity vector distribution

Figures 12 to 15 illustrate the velocity vector distribution on the front faces of containers. It can be seen that the flow tends to penetrate into the spacing between the containers. As dx increases, the flow becomes more streamlined, with higher velocities occurring within the gaps near the first container block. In the absence of gaps between the containers, two characteristic symmetrical vortices are observed in the wake, caused by the separation of airflow at the rear of the superstructure. In contrast, when gaps are introduced between the container blocks, the vortices disappear. Air then flows more freely through the structure, which significantly reduces the formation of the turbulent wake. A region of low velocity is observed at the front face of the containers, and this region tends to shrink as the longitudinal gap dx between the container blocks increases.

Figure 16 shows the average pressure distribution values on the front faces of the ship (front face x = 0, front face of the container blocks x = 0.392 m, and on the front face of the superstructure x = 3.406 m). It is observed that the pressure on the front face of the superstructure decreases as dx increases.

Figure 17 presents the vertical distribution of normalized wind speed above the top of the container blocks, expressed as a function of the dimensionless distance (x/step height). The vertical axis represents the dimensionless height (z/step height) above the top of the container blocks, which is the height of the block containers.

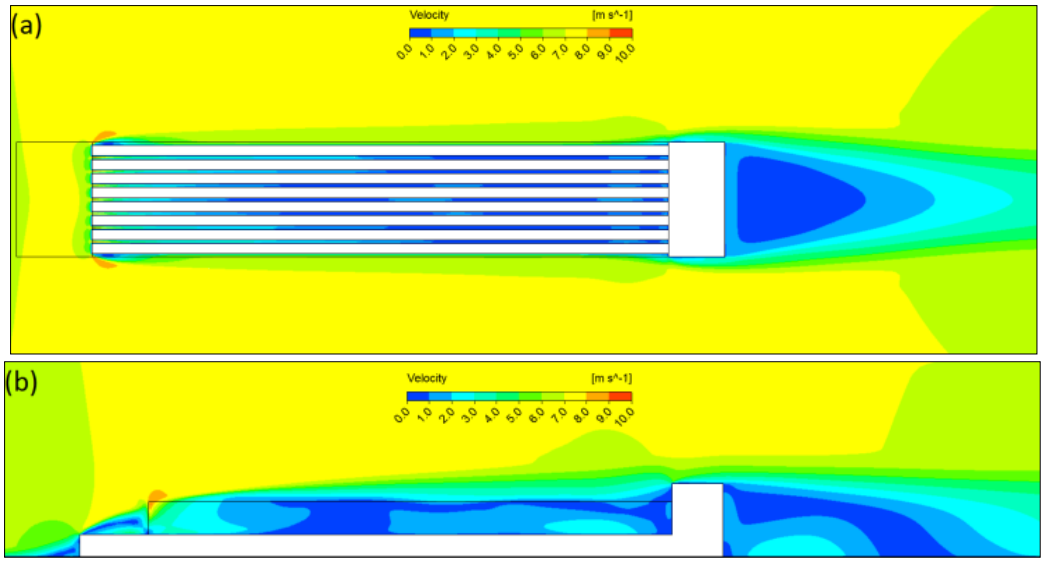

Figure 10. Velocity distribution on the longitudinal (z = 0.222 m) and transverse (y = 0) planes of the container ship for longitudinal container gaps dx = 20 mm

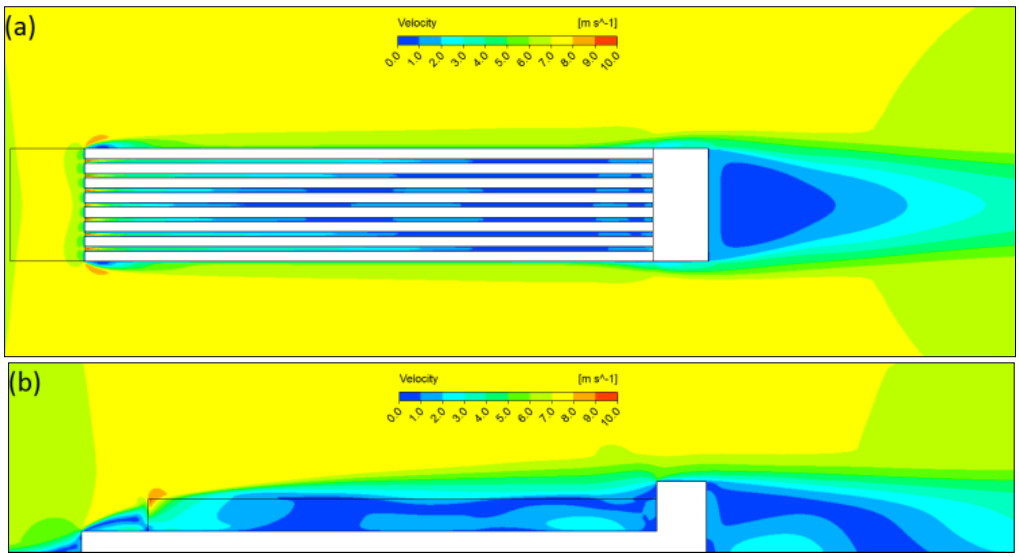

Figure 11. Velocity distribution on the longitudinal (z = 0.222 m) and transverse (y = 0) planes of the container ship for longitudinal container gaps dx = 25 mm

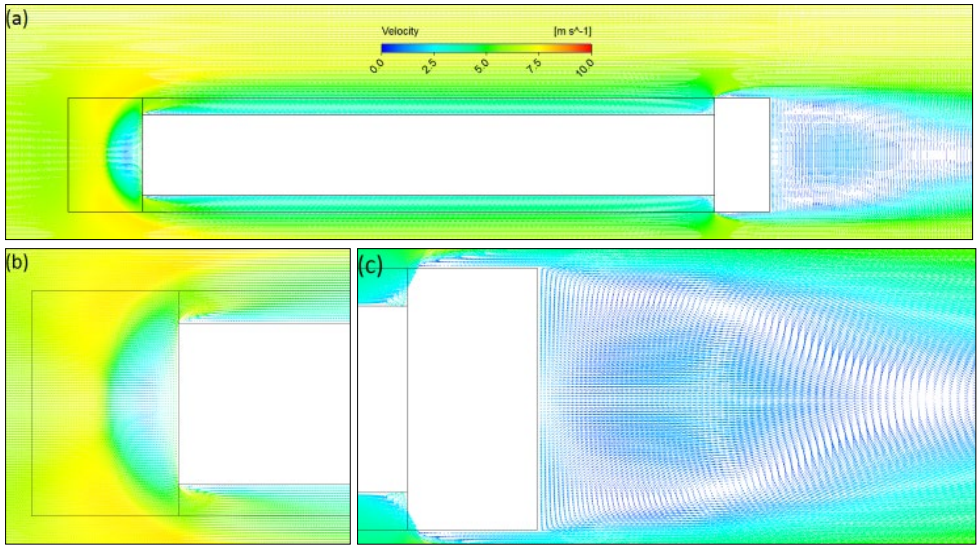

Figure 12. Velocity vector distribution on the longitudinal plane (z = 0.222 m) of the container ship for longitudinal container gaps dx = 0 mm

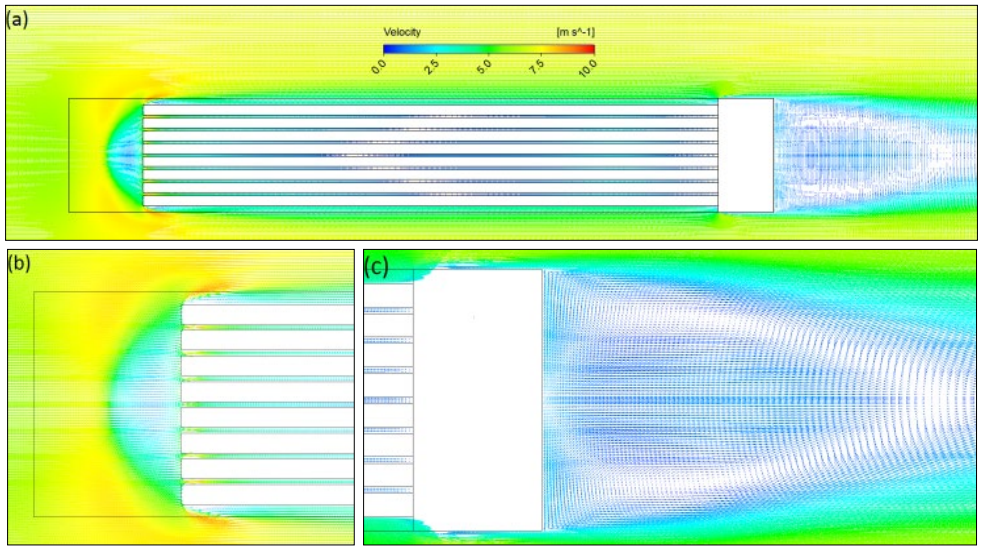

Figure 13. Velocity vector distribution on the longitudinal plane (z = 0.222 m) of the container ship for longitudinal container gaps dx = 15 mm

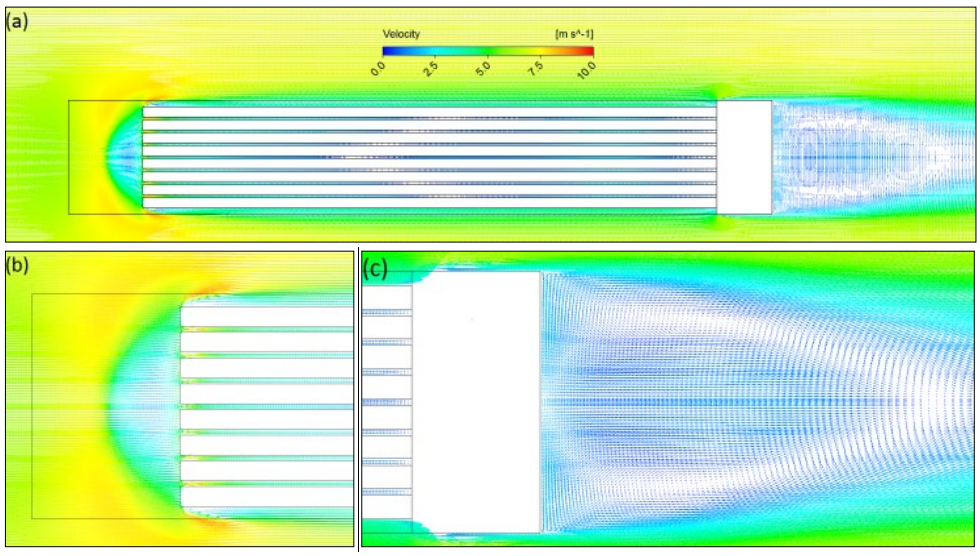

Figure 14. Velocity vector distribution on the longitudinal plane (z = 0.222 m) of the container ship for longitudinal container gaps dx = 20 mm

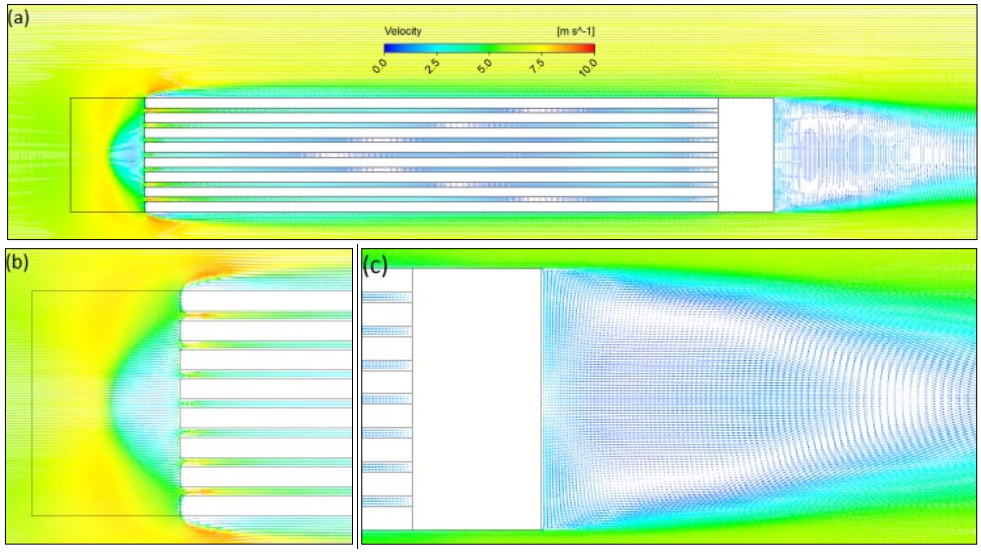

Figure 15. Velocity vector distribution on the longitudinal plane (z = 0.222 m) of the container ship for longitudinal container gaps dx = 25 mm

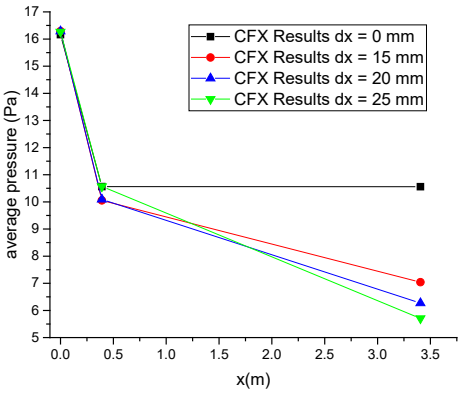

Figure 16. Average pressure distribution values on the front faces of the ship (front face x = 0, front face of the container blocks x = 0.392 m, and front face of the superstructure x = 3.406 m)

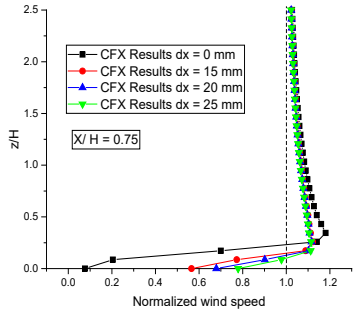

Figure 17. CFD-predicted vertical profiles of normalized wind speed at the leading edge of the container block and at x/H = 0.25 and 0.75

The profiles are presented at dimensionless streamwise positions x/H = 0 (leading edge), 0.25 and 0.75. The dashed line represents a normalized velocity of 1.0, corresponding to the free-stream speed. CFD results obtained in the depression zones showed that the velocity decreases in this zone as dx increases.

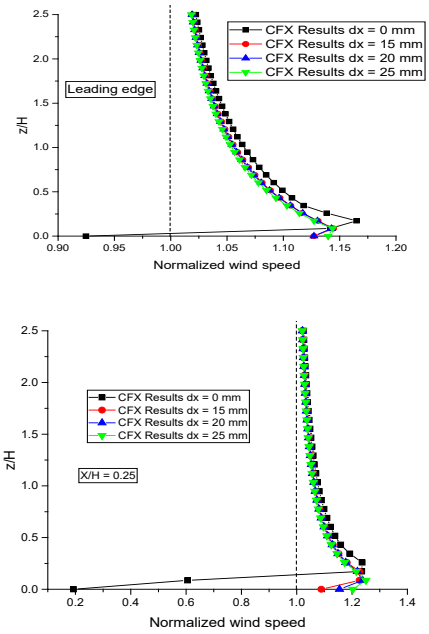

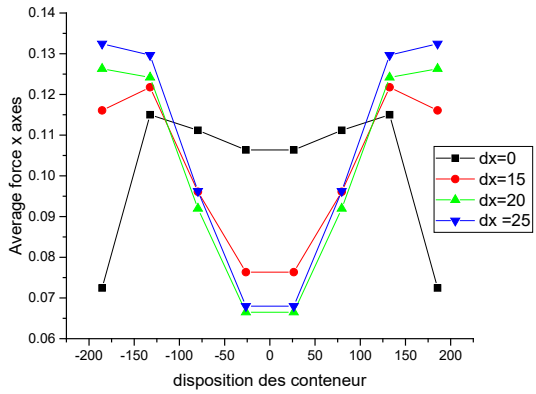

Figure 18. Force distribution on the front faces of the containers

Table 2. Distribution of the force Fx for the longitudinal gaps between containers, dx = 0 mm, dx = 15 mm, dx = 20 mm, and dx = 25 mm, on a container ship

Designation	Validation	Dx = 0 mm	Dx = 15 mm	Dx= 20 mm	Dx = 25 mm
Y^+	273	277	268	264	261
Number of Nodes	10809246	12539721	13051776	12848638	13462834
H	7	7	7	7	7
F_X	4.0736945	4.280713	3.844188	3.789527	3.788696
%			10.2	11.47	11.49

Figure 18 shows the force distribution on the front face of the containers for different configurations. It is observed that for dx = 0, the force tends to be lower on the faces of the end containers, and reaches its minimum value at the middle containers. A similar trend is observed for the other configurations; however, the maximum force is higher at the end containers and decreases to a lower minimum at the middle containers. Moreover, it is noted that as dx decreases, the maximum force also decreases.

Table 2 summarizes the percentage of the Fx force for different configurations, ranging from dx = 0 to dx = 25 mm. It can be observed that as dx increases, the force decreases, with a reduction of 11.49% for dx = 25.

8. CONCLUSION

This study investigates the influence of spacing between containers for different gap sizes dx. The findings indicate that increasing the gap reduces aerodynamic forces. The spacing between the block's containers significantly reduces the formation of a turbulent wake. It is observed that the pressure on the front face of the superstructure decreases as dx increases.

In the absence of gaps, two characteristic symmetrical vortices are observed in the wake; in contrast, when gaps are introduced between the container blocks, the vortices disappear. A reduction in aerodynamic force ranging from 10.2% to 11.49% was observed for gaps between 15 mm and 25 mm in the scaled model of the ship. For a 170 m container ship operating at 7 m/s, this aerodynamic force reduction can lead to fuel savings of approximately 1% and a corresponding reduction in emissions during actual ship operations.

The study is limited by several factors, including the consideration of only a 0° wind angle, steady uniform inflow, neglect of wave effects, and the use of a scaled model. Future work could explore different wind angles, dynamic wind conditions, and comparison with full-scale trials to further validate and extend the findings.

REFERENCES

[1] Majidian, H., Azarsina, F. (2018). Aerodynamic simulation of a containership to evaluate cargo configuration effect on frontal wind loads. China Ocean Engineering, 32(2): 196-205. https://doi.org/10.1007/s13344-018-0021-1

[2] Grlj, C.G., Degiuli, N., Tuković, Ž., Farkas, A., Martić, I. (2023). The effect of loading conditions and ship speed on the wind and air resistance of a containership. Ocean Engineering, 273: 113991. https://doi.org/10.1016/j.oceaneng.2023.113991

[3] Andersen, I.M.V. (2013). Wind loads on post-panamax container ship. Ocean Engineering, 58: 115-134. https://doi.org/10.1016/j.oceaneng.2012.10.008

[4] Deng, R., Song, Z., Ren, H., Li, H., Wu, T. (2022). Investigation on the effect of container configurations and forecastle fairings on wind resistance and aerodynamic performance of large container ships. Engineering Applications of Computational Fluid Mechanics, 16(1): 1279-1304. https://doi.org/10.1080/19942060.2022.2086177

[5] Qiao, D., Ma, N., Gu, X. (2019). Study on wind load characteristics for a container ship under different stacking modes. Chinese Journal of Ship Research, 14(3): 105-115. https://doi.org/10.19693/j.issn.1673-3185.01410

[6] Kim, Y., Kim, K.S., Jeong, S.W., Jeong, S.G., Van, S.H., Kim, Y.C., Kim, J. (2015). Design and performance evaluation of superstructure modification for air drag reduction of a container ship. Journal of the Society of Naval Architects of Korea, 52(1): 8-18. https://doi.org/10.3744/SNAK.2015.52.1.8

[7] Watanabe, I., Van Nguyen, T., Miyake, S., Shimizu, N., Ikeda, Y. (2016). A study on reduction of air resistance acting on a large container ship. In the Eighth Proceedings of the Asia-Pacific Workshop on Marine Hydrodynamics (APHydro), Hanoi, Vietnam, pp. 321-330.

[8] Nguyen, V.T., Le, M.D., Nguyen, V.M., Katayama, T., Ikeda, Y. (2023). Influences of gap flow on air resistance acting on a large container ship. Journal of Marine Science and Engineering, 11(1): 160. https://doi.org/10.3390/jmse11010160

[9] Nguyen, T.V., Ikeda, Y. (2017). Vortex control in gap flow by small appendages to reduce air resistance acting on deck containers of a ship. In Proceedings of the 25th Conference of the Japan Society of Naval Architects and Ocean Engineers, Tokyo, Japan, pp. 335-338. https://doi.org/10.14856/conf.24.0_335

[10] Nguyen, T.V., Shimizu, N., Kinugawa, A., Tai, Y., Ikeda, Y. (2017). Development of practical gap covers to reduce air resistance acting on deck containers of a ship. In Proceedings of the 25th Conference of the Japan Society of Naval Architects and Ocean Engineers, Hiroshima, Japan, pp. 211-216. https://doi.org/10.14856/conf.25.0_211

[11] Moat, B.I., Yelland, M.J., Molland, A.F. (2006). Quantifying the airflow distortion over merchant ships. Part II: Application of the model results. Journal of Atmospheric and Oceanic Technology, 23(3): 351-360. https://doi.org/10.1175/JTECH1859.1

[12] Moat, B.I. (2003). Quantifying the effects of airflow distortion on anemometer wind speed measurements from merchant ships. Ph.D. Thesis, School of Engineering Sciences, University of Southampton, Southampton, United Kingdom.

[13] Janssen, W.D., Blocken, B., van Wijhe, H.J. (2017). CFD simulations of wind loads on a container ship: Validation

and impact of geometrical simplifications. Journal of Wind Engineering & Industrial Aerodynamics, 166: 106-116. https://doi.org/10.1016/j.jweia.2017.03.015

[14] He, N.V., Mizutani, K., Ikeda, Y. (2017). Reducing air resistance acting on a ship by using interaction effects between the hull and accommodation. ASEAN Engineering Journal, 7(1): 1-14. https://doi.org/10.11113/aej.v7.15484

[15] Seok, J., Park, J.C. (2020). Comparative study of air resistance with and without a superstructure on a container ship using numerical simulation. Journal of Marine Science and Engineering, 8(4): 267. https://doi.org/10.3390/jmse8040267

[16] Wang, W., Wu, T., Zhao, D., Guo, C., Luo, W., Pang, Y. (2019). Experimental–numerical analysis of added resistance to container ships under presence of wind–wave loads. PLoS ONE, 14(8): e0221453. https://doi.org/10.1371/journal.pone.0221453

[17] O'Sullivan, N., Landwehr, S., Ward, B. (2015). Air-flow distortion and wave interactions on research vessels: An experimental and numerical comparison. Methods in Oceanography, 12: 1-17. https://doi.org/10.1016/j.mio.2015.03.001

[18] Ricci, A., Janssen, W.D., van Wijhe, H.J., Blocken, B. (2020). CFD simulation of wind forces on ships in ports: Case study for the Rotterdam Cruise Terminal. Journal of Wind Engineering & Industrial Aerodynamics, 205: 104315. https://doi.org/10.1016/j.jweia.2020.104315

[19] Majidian, H., Azarsina, F. (2019). Numerical simulation of container ship in oblique winds to develop a wind resistance model based on statistical data. Journal of International Maritime Safety, Environmental Affairs and Shipping, 2(2): 67-88. https://doi.org/10.1080/25725084.2018.1564471

[20] Ariff, M., Salim, S.M., Cheah, S.C. (2009). Wall y+ approach for dealing with turbulent flow over a surface mounted cube: Part II – high Reynolds number. In Proceedings of the Seventh International Conference on CFD in the Minerals and Process Industries, CSIRO, Melbourne, Australia.

[21] Park, H., Lee, P., Kim, J., Kim, H., Lee, H., Lee, Y. (2024). Study on the estimation method of wind resistance considering self-induced wind by ship advance speed. Journal of Marine Science and Engineering, 12(10): 1694. https://doi.org/10.3390/jmse12101694